



## ORIGINAL ARTICLE

# *Asparagus racemosus* mediated silver chloride nanoparticles induce apoptosis in glioblastoma stem cells *in vitro* and inhibit Ehrlich ascites carcinoma cells growth *in vivo*



Syed Rashel Kabir<sup>a,\*</sup>, Farhadul Islam<sup>a</sup>, Md. Abdul Alim Al-Bari<sup>b</sup>,  
A.K.M. Asaduzzaman<sup>a</sup>

<sup>a</sup> Department of Biochemistry and Molecular Biology, Faculty of Science, University of Rajshahi, Rajshahi 6205, Bangladesh

<sup>b</sup> Department of Pharmacy, Faculty of Science, University of Rajshahi, Rajshahi 6205, Bangladesh

Received 4 February 2022; accepted 24 May 2022

Available online 29 May 2022

## KEYWORDS

Apoptosis;  
Gene expression;  
Cell cycle;  
Cancer prevention;  
Cancer stem cells;  
EAC cells

**Abstract** Glioblastoma multiforme (GBM) is a type of brain tumor that is most aggressive, proliferates rapidly and intensive invasion is governed by cell migration and destruction of the extracellular matrix. In the present study, we evaluated the antiproliferative efficacy of the synthesized silver chloride nanoparticles (AgCl-NPs) from *Asparagus racemosus* root extract against human glioblastoma stem cells (GSCs) and Ehrlich ascites carcinoma (EAC) cells. Biosynthesis of *A. racemosus*-AgCl-NPs was confirmed by color change, UV-visible spectroscopy and characterized by transmitted electron microscope, energy dispersive spectroscopy, x-ray powder diffraction and Fourier-transform infrared spectroscopy. The *A. racemosus*-AgCl-NPs inhibited GSCs and EAC cells growth with the IC<sub>50</sub> values of 4.8 and 4.69 μg/ml, respectively. *A. racemosus*-AgCl-NPs induced apoptosis in GSCs which was confirmed by annexin V/PI assay, various genes expression, and caspase-3 protein expression as detected by the immunofluorometric assay. The expression level of the TLR9, NFκB, TNFα, p21 and IKK genes were increased consequently with the decrease of PARP, EGFR, NOTCH2, mTOR and STAT3 genes in GSCs as examined by real-time PCR. The cell cycle arrest at G<sub>0</sub>/G<sub>1</sub> phase was detected by flow cytometry. In addition, *A. racemosus*-AgCl-NPs caused significant inhibition of EAC cells growth, reduced tumor burden, increased the sur-

\* Corresponding author.

E-mail address: rashelkabir@ru.ac.bd (S.R. Kabir).

Peer review under responsibility of King Saud University.



Production and hosting by Elsevier

vival of EAC-bearing mice and restored the hematological parameters when compared with the control mice. The synthesized AgCl-NPs inhibited the proliferation of GSCs *in vitro* with the induction of apoptosis and inhibited the growth of EAC cells *in vivo* in mice by reducing the tumor burden and increasing the survival periods.

© 2022 The Author(s). Published by Elsevier B.V. on behalf of King Saud University. This is an open access article under the CC BY-NC-ND license (<http://creativecommons.org/licenses/by-nc-nd/4.0/>).

## 1. Introduction

Glioblastoma multiforme (GBM) is the most frequent and the most aggressive grade IV malignant type of primary brain tumor in adults (Ostrom et al., 2015; Roosen et al., 1989). Hallmarks of this aggressive cancer include a heterogeneous mixture of low differentiated neoplastic astrocytes in early-stage and extensive infiltration, as well as strong vascular proliferation into the brain parenchymal niches (Huang et al., 2017; Lee et al., 2017). Over the past decade, thousands of articles reported on the prognosis, treatment response and treatment target of glioblastoma (Ozdemir-Kaynak et al., 2018; Wei et al., 2014). However, till now, for controlling the disease, no remarkable therapeutic options and useful treatments have been referred (Huang et al., 2017; Lee et al., 2017). Thus, a translational new approach is essential for the treatment of these patients.

Nanotechnology-based drug delivery can be one of the emerging and promising techniques (Thuy et al., 2015). Researchers are trying to use metal nanoparticles in the pharmaceutical and biomedical areas as alternative antimicrobial & anticancer agents (Asaduzzaman et al., 2016; Aygün et al., 2020; Baghbani-Arani et al., 2017; Kabir et al., 2020a). The most impressive nanoparticles (NPs) were made from noble metals, particularly silver, gold and platinum. Among them, silver has been attracted due to its tremendous medicinal value to culinary items e.g., disinfection and showing enormous anticancer efficiency. Although several synthesizing techniques are available in nanotechnology-based drug delivery, the biogenic silver-NPs achieved great attention due to their eco-friendliness and the usage of natural resources. Biomolecules that are available in plants, interact with the silver and thereby serve as reducing & capping agents (Ahmed et al., 2016). Recently, researchers found herbal extract-mediated synthesized silver nanoparticles retained potent antiproliferative effects against cancer cells (Antony et al., 2013; Barabadi et al., 2019a; Barua et al., 2013; Firdhouse and Lalitha, 2013; Kabir et al., 2020a, 2020b). The genotoxicity of some biogenic nanoparticles is highly dependent on the biological source, synthesis parameters, applied assay, etc. that varies case-by-case (Barabadi et al., 2019b). Recently, several times higher toxicity of the biogenic silver nanoparticles was reported in cancer cells than normal cells and few of them did not exert any toxicity against the normal cells (Barabadi et al., 2019a, 2018). Recently, we have synthesized Ag/AgCl-NPs from *Geodorum densiflorum* rhizome, *Zizyphus mauritiana* fruit extract and *Kaempferia rotunda* tuberous rhizome extracts that exerted toxic effects against the human glioblastoma stem cancer cells (GSCs), breast cancer cells (MCF-7), human pancreatic cancer cells (BxPC-3) and Ehrlich ascites carcinoma (EAC) cells (Kabir et al., 2020a, 2020b, 2022). In search of the most effective biogenic silver nanoparticles, roots of the *Asparagus racemosus* Wild (family Asparagaceae) were used in the present study and tested against GSCs and EAC cells.

*A. racemosus*, locally known as ‘Satomuli’ is commonly used in the ‘Ayurvedic medicine’ due to its several beneficiary effects. The plant extract is used for the treatment of several diseases and many bioactive compounds (shatavarin IV, lectin, sarsapogenin and diosgenin-derived steroidal constituents) those shown anticancer activities against different cancer cells *in vitro* and *in vivo* were isolated from the root (Bhutani et al., 2018; Kabir et al., 2021; Mitra et al., 2012). However, the anticancer activity of *A. racemosus* or its derivative

nanoparticles against glioblastoma stem cells and EAC cells has never been reported. Therefore, in this manuscript, AgCl-NPs were synthesized from the root extract of *A. racemosus* and characterized using different techniques. Finally, antiproliferative mechanisms were elucidated against GSCs *in vitro* and EAC cells *in vivo* in mice.

## 2. Materials and methods

### 2.1. Chemicals and reagents

The chemicals which were used were purchased from world-leading companies e.g. Gibco, Promega, Amresco, Life technology, Applied biosystem, etc.

### 2.2. Sample preparation

*A. racemosus* roots were purchased from the medicinal village, Natore district, Bangladesh. Around 300 g of the *A. racemosus* roots were washed with deionized water and homogenized with 1 L of 10 mM of Tris-HCl. The homogenate was centrifuged at 10,000g for 30 min at 4 °C and the clear supernatant was collected for the synthesis of silver nanoparticles.

### 2.3. Silver chloride nanoparticles synthesis

To find out the best condition of the synthesis of nanoparticles, 2 ml of supernatant was taken to each of the four test tubes and 0.5 M of AgNO<sub>3</sub> solution was mixed with supernatant of each test tube to reach the final concentration of 1, 2, 3 and 4 mM, and kept under sunlight for 2 h. The samples turned transparent to deep brown color and then analyzed under UV-visible spectroscopy at the range of 250 to 700 nm wavelengths. Based on the maximum peak, 4 mM of AgNO<sub>3</sub> was selected for the synthesis of nanoparticles on a large scale. 1 M of AgNO<sub>3</sub> was mixed with 1 L of supernatant in 4 different beakers at the final concentration of 4 mM and kept in sunlight for 2 h and then centrifuged at 10,000g for 30 min. The pellet was washed three times with deionized water and measured the concentration of the synthesized nanoparticles after lyophilizing part of the colloidal sample.

### 2.4. Characterization of *A. racemosus*-AgCl-NPs

The size and shape were measured by Transmitted Electron Microscope (JEOL, Japan), the presence of elements were analyzed by the energy dispersive spectroscopy (EDX), crystal formation was detected by X-ray powder diffraction (XRD) and the functional groups were determined by Fourier transform infrared spectroscopy (FTIR, Perkin Elmer, Spectrum 100, USA) according to Kabir et al. (Kabir et al., 2020a, 2020b).

### 2.5. Glioblastoma stem cells (GSCs) and EAC cells culture

The human glioma stem cells-3 (GSCs) that was used in this experiment were isolated by the Kunming Institute of Zoology (Dai et al., 2017; Peng et al., 2020). The cells were culture according to Wan Peng et al. (Peng et al., 2020). For the treatment of GSCs with the synthesized *A. racemosus*-AgCl-NPs, at first 6 or 96 well flats bottom cell culture plates were coated with Laminin solution and phosphate buffer saline (1:100) and incubated at 37 °C for 2.0 h. Then PBS and the unbound Laminin were removed from the cell culture petri-dish or culture plates and GSCs in DMEM/F12 medium (Gibco) were seeded and cells were cultured in a 5% CO<sub>2</sub> incubator at 37 °C until cells reached 80–90% confluence. EAC cells were propagated intraperitoneally in our Departmental Research Laboratory biweekly and the cells were collected from a donor Swiss albino mouse bearing 6–7-day-old ascites tumor.

### 2.6. MTS (3-(4,5-dimethylthiazol-2-yl)-5-(3-carboxymethoxyphenyl)-2-(4-sulfophenyl)-2H-tetrazolium) assay

Cytotoxicity was checked by seeding  $2 \times 10^4$  GSCs in each well of a 96 wells cell culture plate as described by Kabir et al. (Kabir et al., 2020b). Cells in DMEM/F12 medium were treated with 2.0 to 8.0 µg/ml concentration of *A. racemosus*-AgCl-NPs for 48 h.  $8 \times 10^4$  EAC cells were added to the serially diluted nanoparticles with DMEM medium of each well of a 96 wells cell culture plate and incubated for 24 h. Finally, aliquot was removed from each well and the cells were incubated with the MTS for 2 to 4 h and the cell proliferation inhibition was calculated as described by Kabir et al. (Kabir et al., 2016). IC<sub>50</sub> values were calculated using the Excel software.

### 2.7. Detection of apoptosis by annexin V/PI assay kit

GSCs ( $2 \times 10^4$ /well) were seeded in a 96 wells plate and 24 h later, cells were treated with 8 µg/ml of *A. racemosus*-AgCl-NPs for 48 h. Then the cells were washed and stained with annexin V and PI (ebioscience, USA) according to the manufacturer's directions. Finally, a fluorescence microscope (Olympus IX71) was utilized for the detection of apoptosis.

### 2.8. Caspase immunofluorescence assay

For immune fluorescence assay, a 96 well cell culture plate was used for seeding GSCs ( $2 \times 10^4$  cells/well). Then the cells were treated with 8 µg/ml of AgCl-NPs for 48 h and then incubated for 1 h with 4% paraformaldehyde for cell fixation. After that 0.1% triton X-100 in PBS was added to the cell for 5 min and washed three times with PBS and 200 µl of 10% goat serum in PBS was added to each well and incubated for 1 h at room temperature. Subsequently, cells were washed with PBS for the removal of serum and 100 µl of the 400 times diluted (by 0.5% tween-20 and 1% BSA in PBS) caspase-3 primary antibody was added and incubated at room temperature for 1 h. Afterward, 0.1% tween-20 in PBS was used to wash the cells for 10 min and 100 µl of Cy3 goat-anti Rabbit IgG antibody (500 times diluted in PBS) was added to each well after removal of the tween-20 and incubated in dark for 2 h at room

temperature. Finally, cells were observed in a fluorescence microscope.

### 2.9. Apoptosis related genes expression by real-time PCR

Around  $32 \times 10^4$  GSCs were seeded in each well of the 6-wells plate and treated with *A. racemosus*-AgCl-NPs (8.0 µg/ml) for 24 h. Then RNA was isolated and cDNA was synthesized according to Kabir et al. (Kabir et al., 2020b). PCR sample was prepared using  $2 \times$  SYBR green master mix as described by the manufacturer (Applied Biosystems). Forward and reverse primers list was given in Table 1. 18s was used as a housekeeping gene. The condition was set up as 50 °C (2 min) and 95 °C (2 min) for 40 cycles 95 °C for 15 sec and 60 °C for 1 min. A Bio-rad thermal cycler (Bio-rad CFX96) was used. Finally, data were analyzed by Double Delta CT methods using MS Excel software.

### 2.10. Cell cycle analysis

Different phases of the cell cycle were analyzed according to Islam et al. (Islam et al., 2018). In short, GSCs were treated with *A. racemosus*-AgCl-NPs (8.0 µg/ml) for 48 h. Then treated and untreated GSCs were detached and fixed with cold 70% ethanol. About 24 h later, ethanol was removed and cells were washed three times with PBS. The cells were treated with RNase A for 30 min at 37 °C. After that, the cells were treated with propidium iodide solution and the cell cycle was analyzed by flow cytometry (BD FACSCalibur, BD Biosciences).

### 2.11. In vivo anticancer activity

The *in vivo* anticancer activity of *A. racemosus*-AgCl-NPs was investigated against EAC cells by examining cell growth inhibition, tumor weight measurement, survival and hematological

**Table 1** List of primers.

NFκB	F	CCAGTATCCCGGTCCAGCTAT
	R	CACGTCCAACACTCACTCCAAGG
TNFα	F	ATTGCCGCAGAAAGTTCTACG
	R	GTCCAGTTTCGTCTTCAGCTC
18 s	F	GTAACCCGTTGAACCCATT
	R	CCATCCAATCGGTAGTAGCG
TLR9	F	CTGCCTTCCTACCCTGTGAG
	R	GGATGCGGTTGGAGGACAA
PARP	F	GGCCTCGGTGGATGGAATG
	R	GCAAACATAACCCGGATAGTCTCT
STAT3	F	CAGCAGCTTGACACACGGTA
	R	AAACACCAAAGTGGCATGTGA
NOTCH2	F	CAACCGCAATGGAGGCTATG
	R	GCGAAGGCACAATCATCAATGTT
EGFR	F	AGGCACGAGTAACAAGCTCAC
	R	ATGAGGACATAACCCAGCCACC
P21	F	TGCAACTACTACAGAACTGCTG
	R	CAAAGTGGTTCGGTAGCCACA
IKK	F	CCCAACGTATGTGGGACCAAG
	R	CACAGCGGTCTTTGCACTTAC
mTOR	F	GCTAGGTGCATTGACATAACAACA
	R	AGTGCTAGTTCACAGATAATGGC

parameter analysis. For cell growth inhibition, EAC cells were collected from EAC-bearing mice in normal saline and  $1 \times 10^6$  cells were injected intraperitoneally in 18 male adult Swiss albino mice ( $25.0 \pm 2.0$  gm). After 24 h of EAC cells inoculation, the mice were randomly distributed into three ( $n = 6$ ) groups and *A. racemosus*-AgCl-NPs injected in the mice of groups I and II at the doses of 2.0 and 4.0 mg/kg/day, respectively, for five consecutive days. Whereas group III serves as non-treated EAC-bearing control. On day seven, EAC cells from all animals were collected in normal saline and viable cells were counted under a light microscope using Trypan blue staining. Finally, the percentages of cell growths were calculated as previously described (Kabir et al., 2012). For tumor burden, survival time and hematological analysis, male adult mice ( $n = 12$ ) were inoculated with EAC cells ( $1 \times 10^6$ ). After 24 h, they were distributed into two groups (group I and group II). Group I received *A. racemosus*-AgCl-NPs (4.0 mg/kg/day) treatment for 10 consecutive days, whereas group II remained as non-treated control. Tumor weights were recorded every second day and the death of each animal was recorded for determining the survival rates of treated and non-treated animals (Kabir et al., 2012). Blood was collected from each animal by the tail puncture on day 10 for hematological parameters analysis.

### 3. Results

#### 3.1. Synthesis of *A. racemosus* mediated of AgCl-NPs and characterization

Development of brown color appeared after the addition of AgNO<sub>3</sub> solution in *A. racemosus* roots extract. The deepness of brown color was raised with the increase of the concentration of AgNO<sub>3</sub> that indicates the formation of *A. racemosus* root extract-mediated AgCl-NPs. The maximum absorbance peak was estimated at 440 nm as shown in Fig. 1A. From 4 L of supernatant, 32 ml of silver chloride nanoparticles was obtained and 1 g of crystalline powder was obtained from 30 ml of the solution. The concentration of the remaining 2 ml solution was 33 mg/ml.

The morphological characterization (such as size and shape) of the *A. racemosus*-AgCl-NPs were determined by TEM. Highly monodispersed spherical particles appeared with an average diameter of approximately 17.0 nm as evaluated by 'ImageJ' software (Fig. 1B). The main elements of the *A. racemosus*-AgCl-NPs were silver and chlorine as observed by EDX (Fig. 1C). The structural characterization showed that the nanoparticles were cubic. The observed reflection peaks and the corresponding crystallographic planes as shown in

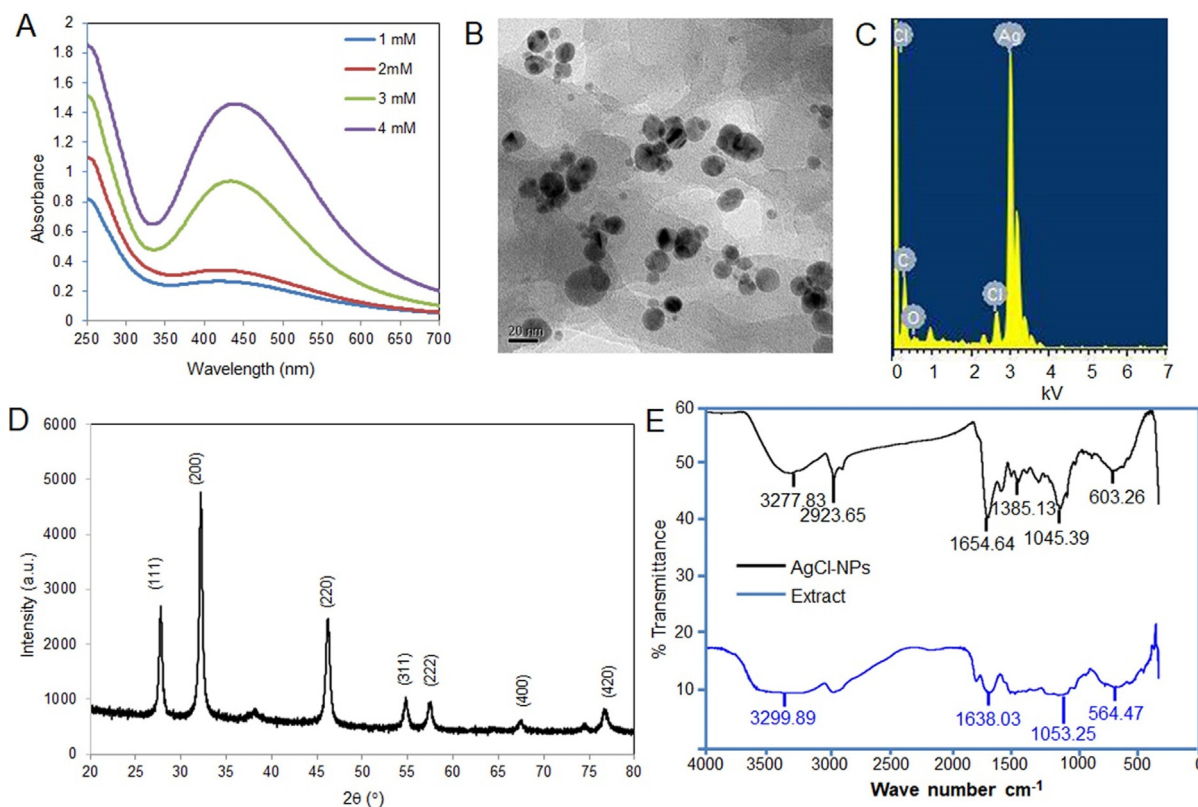


**Fig. 1** Synthesis and characterization of *A. racemosus*-AgCl-NPs. (A) Different spectra indicate the formation of nanoparticles at different concentrations of AgNO<sub>3</sub>. (B) TEM micrograph of the synthesized *A. racemosus*-AgCl-NPs. Morphology showing the *A. racemosus*-AgCl-NPs with different sizes. (C) Detection of the elements in *A. racemosus*-AgCl-NPs by EDX, (D) X-Ray Diffraction pattern (E) FTIR spectrum.

Fig. 1D recognized for the formation of *A. racemosus*-AgCl-NPs (Card no. 00-901-1666). The FTIR spectra for the functional characterization of the *A. racemosus* root extract and *A. racemosus*-AgCl-NPs were presented in Fig. 1E.

### 3.2. Cytotoxic test of *A. racemosus*-AgCl-NPs by MTS assay

GSCs and EAC cells were treated with the *A. racemosus*-AgCl-NPs at the concentration of 2.0 to 8.0  $\mu\text{g/ml}$ . The nanoparticles suppressed the growth of GSCs in a dose-dependent manner. The GSCs growth inhibition was 35%, 50% and 63%, on the other hand, EAC cells growth inhibition was 85%, 55.6% and 8% at concentrations of 2.0, 4.0 and 8.0  $\mu\text{g/ml}$ , respectively (Fig. 2A&B).  $\text{IC}_{50}$  was 4.8  $\mu\text{g/ml}$  for GSCs and 4.69  $\mu\text{g/ml}$  for EAC cells.

### 3.3. Effect of *A. racemosus*-AgCl-NPs on GSCs morphological alteration

After treatment of GSCs with the *A. racemosus*-AgCl-NPs, both early and late apoptotic cells were observed in microscopic images, as shown in Fig. 3. The expression level of active caspase-3 protein was also significantly increased after treatment with *A. racemosus*-AgCl-NPs (Fig. 4).

### 3.4. Effect of *A. racemosus*-AgCl-NPs on the gene expressions of GSCs

After treatment of GSCs with *A. racemosus*-AgCl-NPs for 24 h, the expression level of the TLR9, NF $\kappa$ B, TNF $\alpha$ , p21 and IKK genes were increased while PARP, EGFR, NOTCH2, mTOR and STAT3 genes were decreased as shown in (Fig. 5).

### 3.5. Analysis of cell cycle

Flow cytometry was used to check the effect of *A. racemosus*-AgCl-NPs on the different phases of the cell cycle of GSCs. In the control GSCs, percentages of the G<sub>0</sub>/G<sub>1</sub>, S, and G<sub>2</sub>/M phases were 59.32, 16.51, and 24.17%, respectively. After treatment, the percent of G<sub>0</sub>/G<sub>1</sub> phase increased to 62.77%, with the decrease of S and G<sub>2</sub>/M phases to 13.58% and 23.65%, respectively. The above results indicated that the G<sub>0</sub>/G<sub>1</sub> phase cell cycle arrest in GSCs after treatment with AgCl-NPs as shown in Fig. 6.

### 3.6. AgCl-NPs inhibit EAC cells growth in Swiss albino mice

*A. racemosus*-AgCl-NPs inhibited EAC cells growth significantly in mice. Around 56.7% and 85.75% EAC cells growth inhibition was observed at the doses of 2.0 and 4.0 mg/kg/day, respectively, when compared to that of non-treated control cells (Fig. 7A).

Treatment of EAC-bearing mice with *A. racemosus*-AgCl-NPs for 10 consecutive days at the dose of 4.0 mg/kg/day caused a significant reduction of tumor burden in EAC-bearing mice (Fig. 7B&C). The treatment also increased 69.38% of the life span of the EAC-bearing mice that received *A. racemosus*-AgCl-NPs in the present study (Fig. 7D).

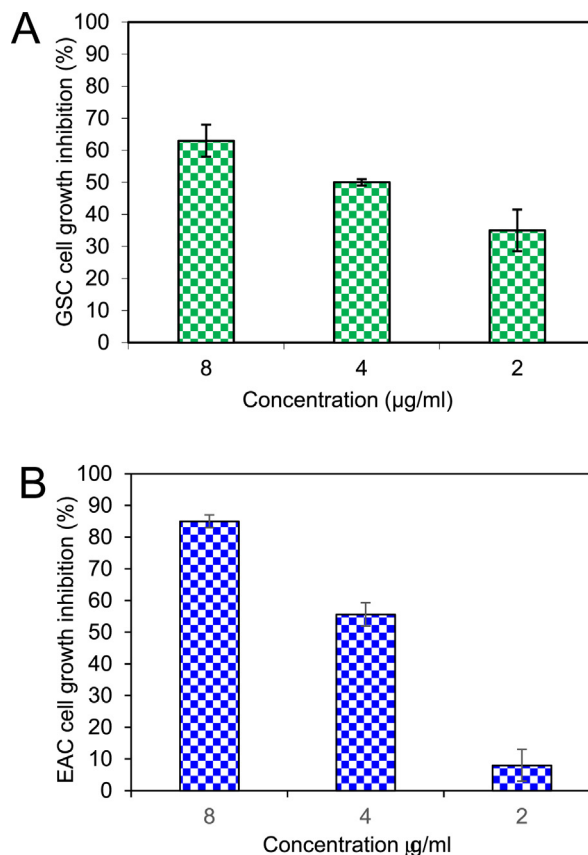
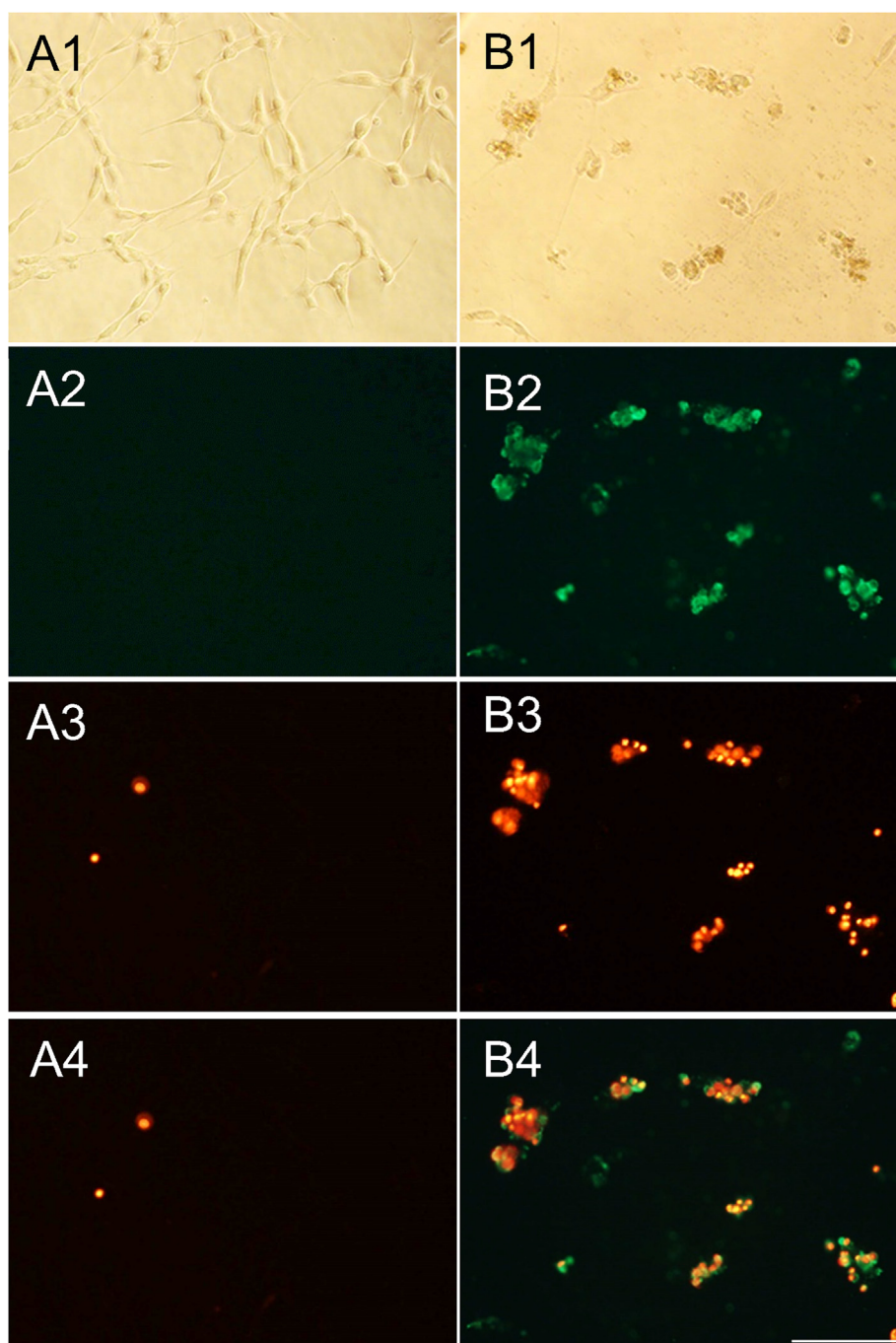


Fig. 2 Antiproliferative activities of *A. racemosus*-AgCl-NPs against GSCs cells (A) and EAC cells (B) *in vitro*.

Additionally, EAC-bearing mice receiving *A. racemosus*-AgCl-NPs treatment restored the blood parameters such as hemoglobin (Fig. 8A), red blood cell and white blood cell (Fig. 8B) counts in comparison to that non-treated EAC-bearing mouse. In EAC-bearing control mice, the hematological parameters deteriorate with the burden of tumor in comparison to that of normal mice. We have noted that treatment of EAC-bearing mice with AgCl-NPs reverse back the deteriorate parameters to the normal levels (Fig. 8A&B).

## 4. Discussion

Various cancer therapeutic agents stimulate cell apoptosis as the most efficient method for the treatment of cancer (Yang et al., 2015). Recently, the apoptotic inducers derived from phytochemicals have attracted much attention to researchers due to the less toxic effects than those of radiation and chemically synthesized chemotherapeutic agents. For this purpose, we attempted to synthesize silver nanoparticles from *Zizyphus mauritiana* fruit extract, *Kaempferia rotunda* tuberous rhizome and *Geodorum densiflorum* rhizome extracts. At that time, we obtained a mixture of AgNPs and AgCl-NPs from the extracts (Kabir et al., 2020a, 2020b, 2022). This time only AgCl-NPs were synthesized from *A. racemosus* roots extract and the formation of the nanoparticles/complex was confirmed preliminary from the deep brown color and the absorbance peaks at 440 nm that occurred for the surface plasmon resonance (Padalia et al., 2015; Singh et al., 2014).



**Fig. 3** Induction of apoptosis in GSCs. (A1) and (B1) control and treat GSCs cells, respectively (bright field microscopic view). (A2) and (B2) fluorometric view of control and treated GSCs after staining with annexin V. (A3) and (B3) fluorometric view of control and treated GSCs after staining with PI; (A4) representing merged of (A2) and (A3) and (B4) representing merged of (B2) and (B3) respectively. The green color indicates the early and red indicates the late apoptotic cells. The image was captured at 40x magnification and the solid bar indicated 20  $\mu$ m.

Like most plant-mediated AgNPs, (Ahmed et al., 2016) highly monodispersed spherical particles appeared with an average diameter of approximately 17.0 nm. The crystalline system of the *A. racemosus*-AgCl-NPs was cubic, as confirmed by XRD. AgCl-NPs can be formed in different manners. In the present study, the formation of the AgCl-NPs can be explained as two steps process (Kang et al., 2016). At first, AgCl is

formed by reacting Ag ions and chloride ions of the Tris-HCl buffer. Then *A. racemosus*-AgCl-NPs are formed by stabilizing the AgCl with different bioactive compounds of the *A. racemosus* root extract. FTIR peaks indicated the possibility of the content of several functional groups e.g. alcohols, phenols, proteins, enzymes, alkenes, esters or polysaccharides in the *A. racemosus*-AgCl-NPs.

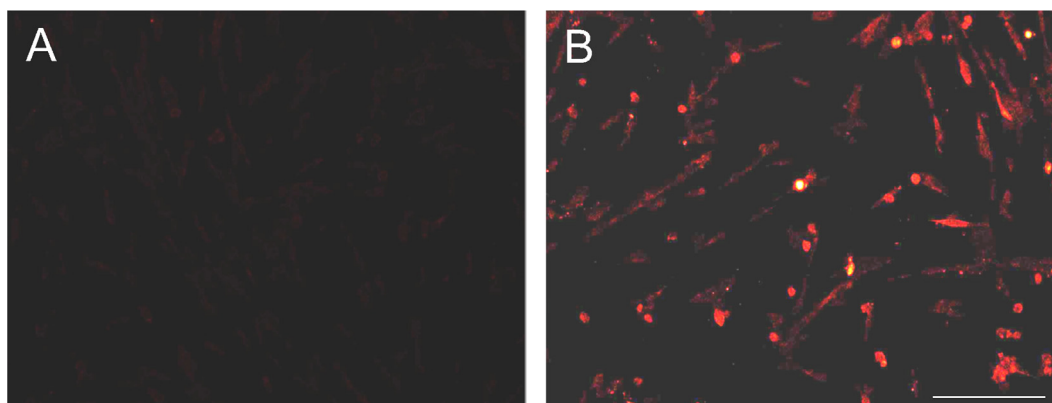


**Fig. 4** Immunofluorometric assay of the *A. racemosus*-AgCl-NPs against GSCs. (A) control GSCs and (B) treated GSCs. The image was captured at 40x magnification and the solid bar indicated 20  $\mu$ m.

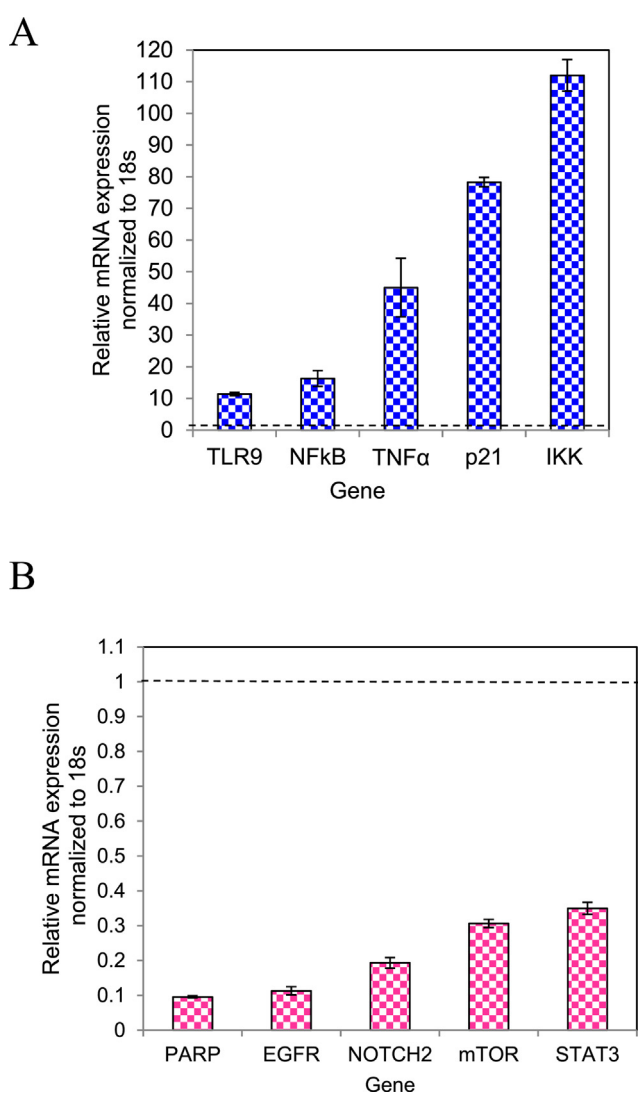


**Fig. 5** Assessment of gene expression levels. (A) expression of TLR9, NFkB, TNF $\alpha$ , p21, IKK, (B) expression of PARP, EGFR, NOTCH2, mTOR and STAT3 genes after treatment of GSCs with *A. racemosus*-AgCl-NPs. A dashed line (black) indicates 1.0 expression level.

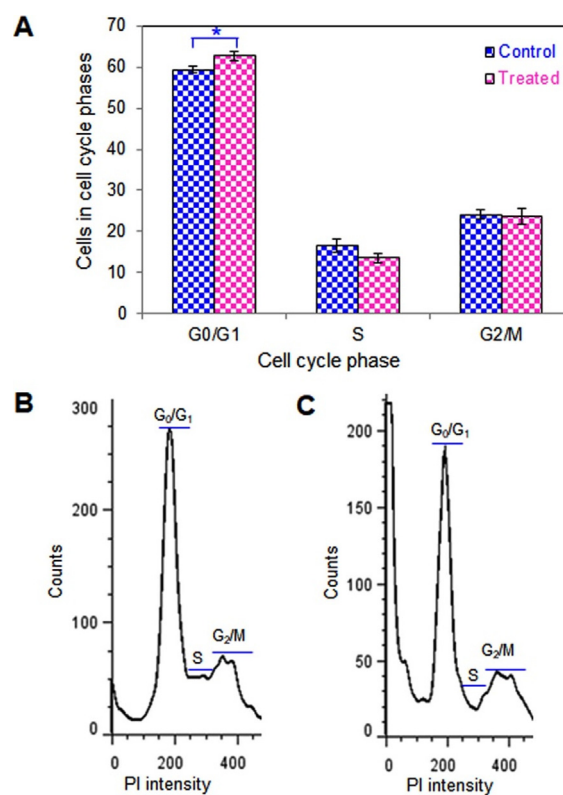


**Fig. 6** Effects of the AgCl-NPs on the cell cycle phases of GSCs. (A) The percentages of each cell cycle were analyzed based on mean values obtained from three independent experiments. (B) is representing the histogram of control GSCs and (C) after treatment with *A. racemosus*-AgCl-NPs. (n = 3, mean  $\pm$  SD). \*p < 0.05.

Glioblastoma multiforme is the primary malignant brain tumor in humans, with a high morbidity rate and under standard treatment, the average overall survival time is approximately 14.6 months and <10% of patients survive around 5 years (Roger Stupp et al., 2009). Recently, CSCs have been identified in these tumors and named glioma stem cells (GSCs) (Sattiraju A et al., 2017). Since GBM is a highly vascularized tumor, it was speculated that GSCs might depend on a similar

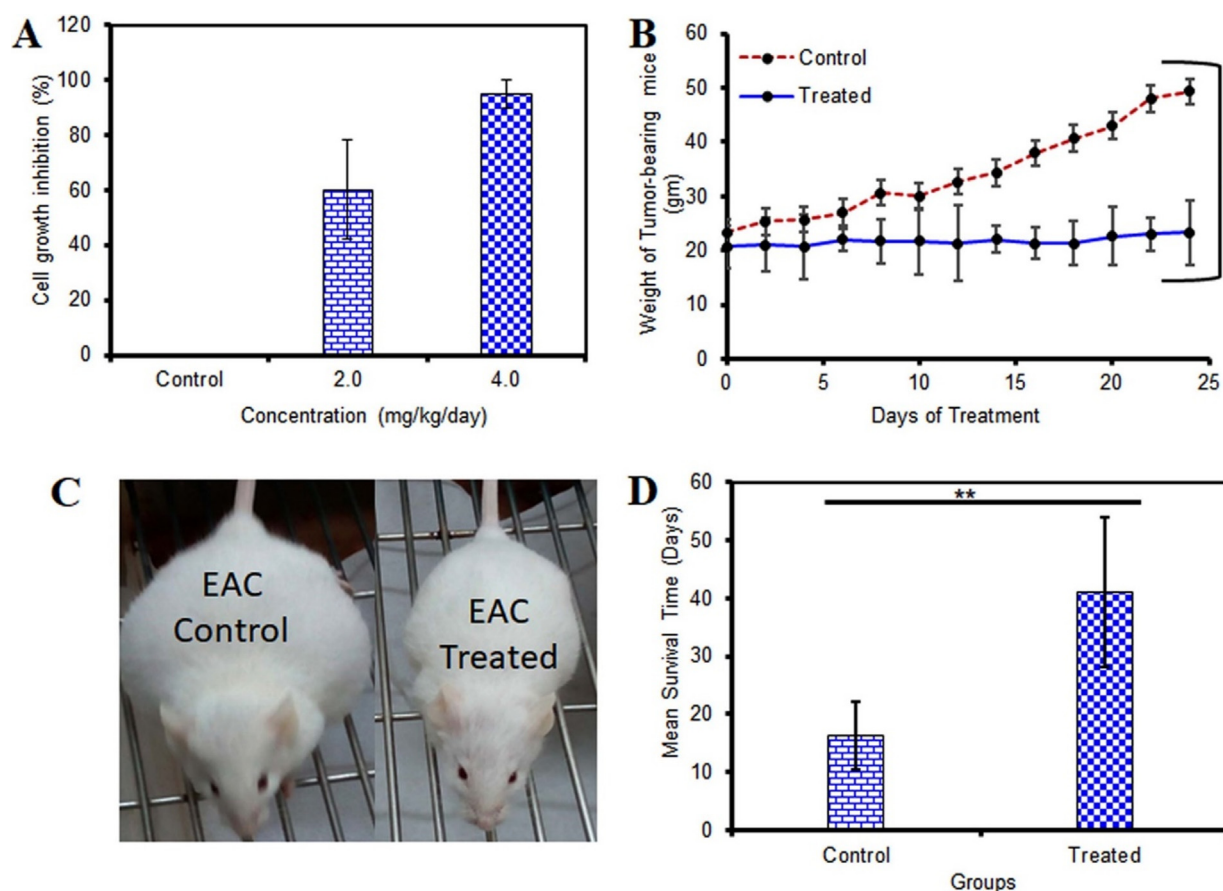


**Fig. 7** In vivo anticancer activity of *A. racemosus*-AgCl-NPs against EAC cells. A) Percentages of EAC cells growth inhibition at the doses of 2.0 and 4.0 mg/kg/day following 5 consecutive days of treatment. B) Tumour weight of EAC-bearing mice receiving *A. racemosus*-AgCl-NPs and control mice. C) *A. racemosus*-AgCl-NPs treated and untreated EAC bearing mice on the 22nd day of EAC inoculation. D) Percentage of the increased life span of EAC-bearing mice receiving treatment and non-treated animals.. (n = 6, mean  $\pm$  SD). \*\*p < 0.01, \*\*\*\*p < 0.0001.

niche as neural stem cells (Sattiraju A et al., 2017). Various mechanisms, including genetics, epigenetics, metabolism, cellular microenvironment, niche factors, and the host immune system all regulate GSCs (Lathia et al., 2015; Wang et al., 2018). The GSCs seem to have cell renewal properties, and autophagy resists chemotherapy and differentiates to additional glioma cells, suspecting them the main mediators for tumor regrowth after treatment (Jiapaer et al., 2018; Louis, 2006). Several molecular resistance mechanisms of GSCs to therapies are dependent on alterations of different gene expressions which in turn underlie GBM pathogenesis (Lathia et al., 2015). Thus, it suggests that several therapeutic combination approaches are being pursued against these GSCs resistant mechanisms.

To evaluate the anticancer properties of the *A. racemosus*-AgCl-NPs, cytotoxicity against GSCs, was checked by MTS assay (at the doses of 2, 4, 8, 16 and 32  $\mu$ g/ml). However, results of the higher doses (16, and 32  $\mu$ g/ml) were not shown in the present study as growth inhibition of GSCs was not significantly higher relative to the dose of 8  $\mu$ g/ml. GSCs were sensitive toward- the synthesized nanoparticles and the proliferation was inhibited in a dose-dependent way. The cell proliferation inhibition was due to the induction of apoptosis confirmed by FITC-annexin V/PI staining and observed the remarkable increase of caspase-3 protein expres-

sion determined by immunofluorescence assay. Various genes are associated with this apoptotic cell death and any modulation of these genes by cell surface receptor inhibitors or kinase inhibitors may inhibit GSC growth and renewal (Cheng et al., 2015). For example, the classical type of GBM is particularly characterized by the amplification of epidermal growth factor receptor (EGFR), which seems to be exclusively a mutated form of TP53 (Eskilsson et al., 2018; Figueroa et al., 2017). NOTCH, a neural stem cell marker is also up-regulated in this classical subtype of GBM (Brennan et al., 2009). EGFR activation and NOTCH signaling enhance GSC proliferation as well as the development of tumorigenesis through the activation of  $\beta$ -catenin. Here, *A. racemosus*-AgCl-NPs down-regulated EGFR and NOTCH2 expression, whose consequence effects might be the induction of apoptosis in GSCs. Thus, targeting these signaling pathways in GSCs would be helpful for the treatment of glioblastoma. Several studies reported the correlation between the GSCs and STATs expression (Sherry et al., 2009). STAT3 plays an essential role in the survival, invasion, and promotion of tumor cell proliferation, angiogenesis and pre-metastatic niche formation (Cao et al., 2010; Wang et al., 2009). Recently, it was reported that a small molecule WP1193, induced apoptosis in glioblastoma stem-like cells by inhibiting JAK2/STAT3 pathway and promoting cell-

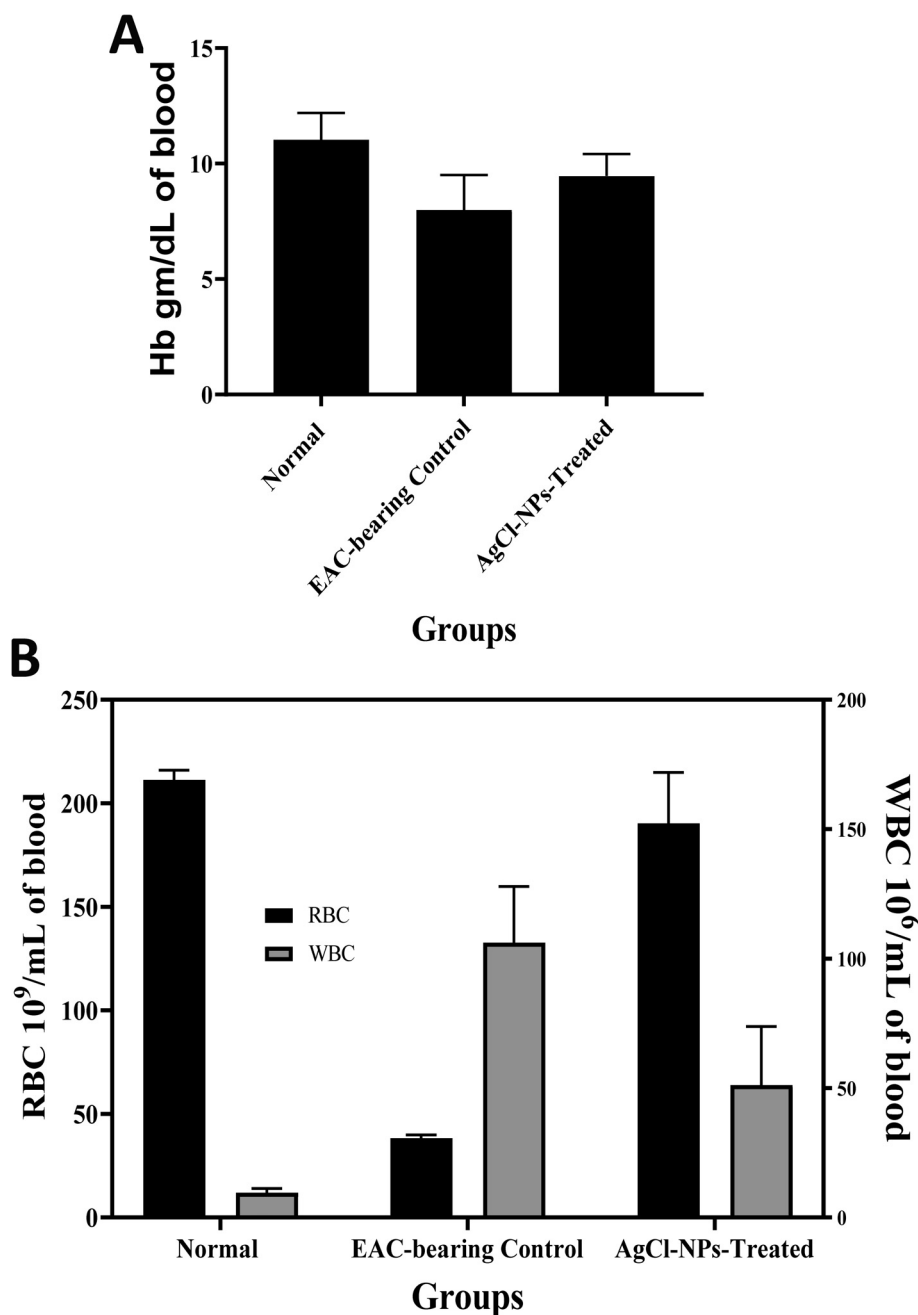


**Fig. 8** Protective effects of *A. racemosus*-AgCl-NPs in EAC-bearing mice. A) Restoration of hemoglobin levels in EAC-bearing mice treated with *A. racemosus*-AgCl-NPs. B) Effects of *A. racemosus*-AgCl-NPs in EAC-bearing mice on RBC and WBC counts. *A. racemosus*-AgCl-NPs treatment reverses the blood cell counts to normal levels.

cycle arrest (Sai et al., 2012). Another report stated that a PARP inhibitor ABT-888, with TMZ and radiation, increases apoptosis in GBM cells (Barazzuol et al., 2013). Here, the anti-apoptotic STAT3 and PARP genes' expression was also down-regulated after *A. racemosus*-AgCl-NPs treatment. Consequently, caspase-3 protein expression was increased and the DNA repair mechanism led by PARP was inhibited. Thus, this strategy that blocks EGFR, NOTCH2, STAT3 and PARP pathways may prove more efficacious for sustained cancer treatment. The expression level of mTOR was also decreased that also supporting the induction of apoptosis.

After treatment of GSCs with the *A. racemosus*-AgCl-NPs, the expression of the toll-like receptor gene TLR9, Nuclear Factor Kappa B Subunit-1 NF- $\kappa$ B, tumor necrosis factor- $\alpha$  TNF $\alpha$ , an inhibitor of nuclear factor kappa-B kinase subunit beta IKK and p21 genes were increased significantly. In GSCs, cell proliferation, invasion, cell cycle progression and apoptosis are regulated by the NF- $\kappa$ B family members (Kim et al., 2016; Li et al., 2015; Yang et al., 2017; Zanotto-Filho et al., 2017). I $\kappa$ B $\alpha$  is the light polypeptide inhibitory gene of the nuclear factor of kappa and the phosphorylation of the gene caused the typical activation of NF- $\kappa$ B(p65) pathway

(Patil et al., 2010). IKK $\alpha/\beta$  phosphorylation degrades I $\kappa$ B $\alpha$  that leads to the release of p65 & p50 and evoking the gene transcription by trafficking into the nucleus (Häcker and Karin, n.d.; Patil et al., 2010). Phosphorylation of IKK increased by the TNF $\alpha$  that causing the decreased level of I $\kappa$ B $\alpha$  consequently increasing the level of nuclear p65 (Gupta et al., 2013). TLRs play a role in the transcription of the NF- $\kappa$ B gene and activate pro-inflammatory cytokines, such as IL6 and TNF $\alpha$  through the adaptor molecule MyD88 (Medzhitov, 2001; Pasare and Medzhitov, 2005). NF- $\kappa$ B plays an anti-apoptotic and pro-apoptotic regulatory factor that is depending on the apoptotic stimulus (Kaltschmidt et al., 2000; Lin et al., 1999). Induction of apoptosis with the several-fold increase of NF- $\kappa$ B may state the role of pro-apoptotic genes. In the present study, *A. racemosus*-AgCl-NPs may cause activation of TNF $\alpha$  directly and/or through TLR9 that activated NF- $\kappa$ B by activating IKK and finally, DNA breakdown occurred. The expression level of the DNA repair gene PARP decreases due to the over-expression of caspase-3 protein. After treatment of GSCs with the *A.*

*racemosus*-AgCl-NPs, G<sub>0</sub>/G<sub>1</sub> cell cycle was arrested, supported by the overexpression of p21 gene. The caspase-3 protein and all gene expression data were pictorially represented in Fig. 9.

In addition, the *A. racemosus*-AgCl-NPs significantly inhibited EAC cells proliferation *in vitro* and also inhibited the EAC cell growth, reduced tumor growth rate and burden, increased the survival and life span of tumor-bearing animals and restored the perturbed hematological parameters when compared with the non-treated control animals. These are the hallmark properties of potential and effective chemotherapeutic agents (Islam et al., 2012; Islam et al., 2015). In our previous *K. rotunda*-mediated Ag/AgCl-NPs inhibited 32.3% and 55% of EAC cells growth *in vivo* in mice at 6 and 12 mg/kg/day doses, respectively, *Z. mauritiana*-mediated Ag/AgCl-NPs inhibited only 20% of EAC cells growth at 12 mg/kg/day dose (Kabir et al., 2020b) and *Hypnea musciformis*-mediated Ag/AgCl-NPs inhibited 22.83% and 51% of the EAC cell growth *in vivo* in mice when administered 1.5 and 3.0 mg/kg/day (i.p.), respectively, for 5 consequent days (Ghose et al., 2022). While in the present investigation 85.75% EAC cells

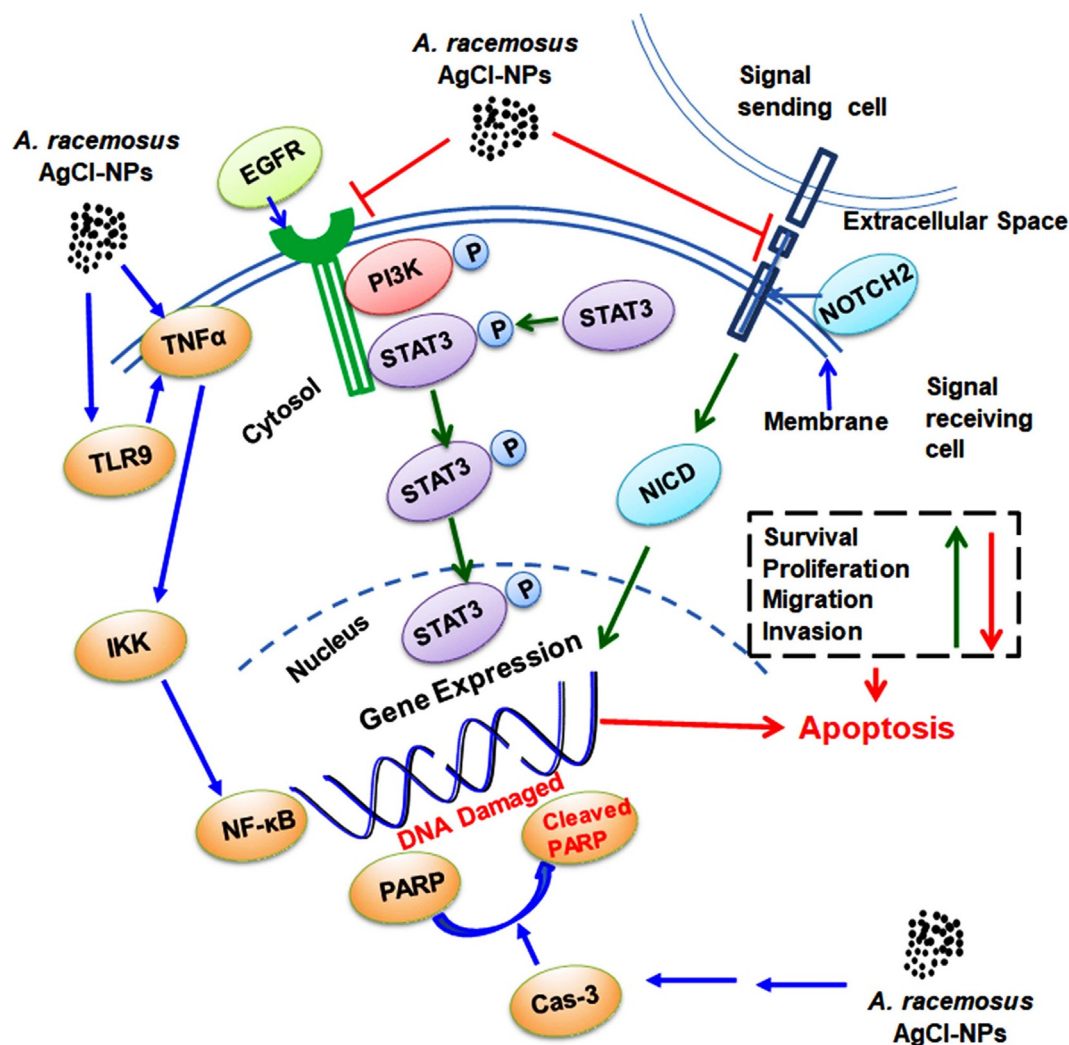


Fig. 9 The possible schematic representation of AgCl-NPs mediated apoptosis and growth inhibition of GSCs.

growth inhibition was observed only at 4 mg/Kg/day doses. That indicated the synthesized nanoparticles are more effective than previously reported nanoparticles and less effective than *G. densiflorum*-Ag/AgCl-NPs that inhibited 95% EAC cells growth at the dose of 4 mg/Kg/day (Kabir et al. 2022). In cancer patient, the hemoglobin and RBC decreased with the increase of WBC. In the present study for the first time, we are reporting the synthesized nanoparticles increased the hemoglobin level and RBC towards the normal consequently in the decrease of WBC. After treatment with *A. racemosus*-AgCl-NPs, the tumor volume remained near to the normal mice while the weight of the control EAC-bearing mice significantly increased with the survival time.

## 5. Conclusion

The synthesized *A. racemosus*-AgCl-NPs supplementation inhibited proliferation of GSC cell *in vitro* and EAC cells both *in vitro* and *in vivo* significantly. The nanoparticles induce apoptosis of GSC cells by arresting cells at G<sub>0</sub>/G<sub>1</sub> phase of the cell cycle via modulating the expression of cellular growth, kinetics, proliferation, survival and death-related genes. Whereas, a significant reduction of tumor burden and increased life-span (*i.e.* survival) of tumor-bearing mice along with restoration of the hematological parameter followed by *A. racemosus*-AgCl-NPs treatment indicated strong anticancer activity of the nanoparticles. Therefore, results from this study implied that *A. racemosus*-AgCl-NPs have potential anticancer properties, which could provide a new resource to designate an effective chemotherapeutic agent.

## Declaration of Competing Interest

The authors declare that they have no known competing financial interests or personal relationships that could have appeared to influence the work reported in this paper.

## Acknowledgment

GSCs related to all works were done by the first author at the Kunming Institute of Zoology, China as a Visiting Scientist under the CAS-PIFI fellowship (Award No. 2017 VBB0001) where Professor Zhao Xudong provided laboratory facilities as a former Faculty member and was not interested to be an author. The rest of the works were done under the financial support of the Ministry of Science and Technology (Grant no:39.009.002.01.00.057.2015-2016/922/Phys-362), Bangladesh.

## Experimental animals and ethical clearance

A total of 36 Swiss albino mice (males, 8 weeks old, 22–25 g weight) were obtained from the animal house of the Pharmacy Department, Jahangirnagar University, Dhaka and were housed in cages (6 mice/cage) with free access to food and water. All animals were kept under a 12-h/12-h light/dark cycle (lights on at 6:00 a.m.). The animals were treated according to the ethical principles for animal experimentation according to protocols approved by the Institutional Animal, Medical Ethics, Bio-safety and Bio-security Committee (IAMEBBC) for Experimentations on Animals, Human, Microbes and Living Natural Sources Institute of Biological Sciences (IBSc), the

University of Rajshahi, Bangladesh (approved certificate No. 293(13)320-IAMEBBC/IBSc).

## References

- Ahmed, S., Ahmad, M., Swami, B., Ikram, S., 2016. A review on plants extract mediated synthesis of silver nanoparticles for antimicrobial applications: a green expertise. *J. Adv. Res.* 7, 17–28. <https://doi.org/10.1016/j.jare.2015.02.007>.
- Antony, J.J., Ali, M., Sithika, A., Joseph, T.A., Suriyakalaa, U., Sankarganesh, A., Siva, D., Kalaiselvi, S., Achiraman, S., 2013. *In vivo* antitumor activity of biosynthesized silver nanoparticles using *Ficus religiosa* as a nanofactory in DAL induced mice model. *Colloids Surf. B Biointerfaces* 108, 185–190. <https://doi.org/10.1016/j.colsurfb.2013.02.041>.
- Asaduzzaman, A.K.M., Chun, B.-S., Kabir, S.R., 2016. Vitis vinifera Assisted Silver Nanoparticles with Antibacterial and Antiproliferative Activity against Ehrlich Ascites Carcinoma Cells. *J. Nanoparticles* 2016, 1–9. <https://doi.org/10.1155/2016/6898926>.
- Aygün, A., Özdemir, S., Gülcan, M., Cellat, K., Şen, F., 2020. Synthesis and characterization of Reishi mushroom-mediated green synthesis of silver nanoparticles for the biochemical applications. *J. Pharm. Biomed. Anal.* 178. <https://doi.org/10.1016/j.jpba.2019.112970>.
- Baghbani-Arani, F., Movagharnia, R., Sharifian, A., Salehi, S., Shandiz, S.A.S., 2017. Photo-catalytic, anti-bacterial, and anti-cancer properties of phyto-mediated synthesis of silver nanoparticles from *Artemisia tournefortiana* Rchb extract. *J. Photochem. Photobiol. B Biol.* 173, 640–649. <https://doi.org/10.1016/j.jphotobiol.2017.07.003>.
- Barabadi, H., Alizadeh, A., Ovais, M., Ahmadi, A., Shinwari, Z.K., Saravanan, M., 2018. Efficacy of green nanoparticles against cancerous and normal cell lines: A systematic review and meta-analysis. *IET Nanobiotechnol.* 12, 377–391. <https://doi.org/10.1049/iet-nbt.2017.0120>.
- Barabadi, H., Mahjoub, M.A., Tajani, B., Ahmadi, A., Junejo, Y., Saravanan, M., 2019a. Emerging Theranostic Biogenic Silver Nanomaterials for Breast Cancer: A Systematic Review. *J. Clust. Sci.* 30, 259–279. <https://doi.org/10.1007/s10876-018-01491-7>.
- Barabadi, H., Najafi, M., Samadian, H., Azarnezhad, A., Vahidi, H., Mahjoub, M.A., Koohiyani, M., Ahmadi, A., 2019b. A systematic review of the genotoxicity and antigenotoxicity of biologically synthesized metallic nanomaterials: Are green nanoparticles safe enough for clinical marketing? *Medicina (Kaunas)*. 55, 439. <https://doi.org/10.3390/medicina55080439>.
- Barazzuol, L., Jena, R., Burnet, N.G., Meira, L.B., Jeynes, J.C.G., Kirkby, K.J., Kirkby, N.F., 2013. Evaluation of poly (ADP-ribose) polymerase inhibitor ABT-888 combined with radiotherapy and temozolomide in glioblastoma. *Radiat. Oncol.* 8, 1–11. <https://doi.org/10.1186/1748-717X-8-65>.
- Barua, S., Konwarh, R., Bhattacharya, S.S., Das, P., Devi, K.S.P., Maiti, T.K., Mandal, M., Karak, N., 2013. Non-hazardous anticancerous and antibacterial colloidal “green” silver nanoparticles. *Colloids Surf. B Biointerfaces* 105, 37–42. <https://doi.org/10.1016/j.colsurfb.2012.12.015>.
- Bhutani, K.K., Linder, S., Bhutani, K.K., Paul, A.T., Fayad, W., Linder, S., 2018. Apoptosis inducing activity of steroidal constituents from *Solanum xanthocarpum* and *Asparagus racemosus*. *Phytomedicine* 17, 789–793. <https://doi.org/10.1016/j.phymed.2010.01.017>.
- Brennan, C., Momota, H., Hambarzumyan, D., Ozawa, T., Tandon, A., Pedraza, A., Holland, E., 2009. Glioblastoma Subclasses Can Be Defined by Activity among Signal Transduction Pathways and Associated Genomic Alterations. *PLoS ONE* 4. <https://doi.org/10.1371/journal.pone.0007752> e7752.
- Cao, Y., Lathia, J.D., Eyler, C.E., Wu, Q., Li, Z., Wang, H., McLendon, R.E., Hjelmeland, A.B., Rich, J.N., 2010. Erythropoi-

- etin receptor signaling through STAT3 Is required for glioma stem cell maintenance. *Genes Cancer* 1, 50–61. <https://doi.org/10.1177/1947601909356352>.
- Cheng, P., Phillips, E., Kim, S.-H., Taylor, D., Hielscher, T., Puccio, L., Hjelmeland, A.B., Lichter, P., Nakano, I., Goidts, V., 2015. Kinome-wide shRNA screen identifies the receptor tyrosine kinase AXL as a key regulator for mesenchymal glioblastoma stem-like cells. *Stem Cell Rep.* 4, 899–913. <https://doi.org/10.1016/j.stemcr.2015.03.005>.
- Dai, Z., Li, S.R., Zhu, P.F., Liu, L., Wang, B., Liu, Y.P., Luo, X.D., Zhao, X.D., 2017. Isocostunolide inhibited glioma stem cell by suppression proliferation and inducing caspase dependent apoptosis. *Bioorg. Med. Chem. Lett.* 27, 2863–2867. <https://doi.org/10.1016/j.bmcl.2017.04.075>.
- Esilsson, E., Røslund, G.V., Solecki, G., Wang, Q., Harter, P.N., Graziani, G., Verhaak, R.G., Winkler, F., Bjerkvig, R., Miletic, H., 2018. EGFR heterogeneity and implications for therapeutic intervention in glioblastoma. *Neuro. Oncol.* 20, 743–752. <https://doi.org/10.1093/neuonc/nox191>.
- Islam, F., Khatun, H., Ghosh, S., Ali, M.M., Khanam, J.A., 2012. Bioassay of Eucalyptus extracts for anticancer activity against Ehrlich ascites carcinoma (eac) cells in Swiss albino mice. *Asian Pac. J. Trop. Bio.* 2, 394–398. [https://doi.org/10.1016/S2221-1691\(12\)60063-X](https://doi.org/10.1016/S2221-1691(12)60063-X).
- Islam, F., Khanam, J.A., Khatun, M., Zuberi, N., Khatun, L., Kabir, S.R., Reza, M.A., Ali, M.M., Rabbi, M.A., Gopalan, V., Lam, A. K., 2015. A p-menth-1-ene-4,7-diol (EC-1) from Eucalyptus camaldulensis Dnh. triggers apoptosis and cell cycle changes in Ehrlich ascites carcinoma cells. *Phytother. Res.* 29, 573–581. <https://doi.org/10.1002/ptr.5288>.
- Figuerola, J.M., Skog, J., Akers, J., Li, H., Komotar, R., Jensen, R., et al, 2017. Detection of wild-type EGFR amplification and EGFRvIII mutation in CSF-derived extracellular vesicles of glioblastoma patients. *Neuro. Oncol.* 19, 1494–1502. <https://doi.org/10.1093/neuonc/nox085>.
- Firdhouse, M.J., Lalitha, P., 2013. Biosynthesis of silver nanoparticles using the extract of *Alternanthera sessilis*-antiproliferative effect against prostate cancer cells. *Cancer Nanotechnol.* 4, 137–143. <https://doi.org/10.1007/s12645-013-0045-4>.
- Ghose, R., Asaduzzaman, A.K.M., Hasan, I., Kabir, S.R., 2022. Hypnea musciformis-mediated Ag/AgCl-NPs inhibit pathogenic bacteria, HCT-116 and MCF-7 cells' growth in vitro and Ehrlich ascites carcinoma cells in vivo in mice. *IET Nanobiotechnol* 16 (2), 49–60. <https://doi.org/10.1049/nbt2.12075>.
- Gupta, P., Dixit, D., Sen, E., 2013. Oncrasin targets the JNK-NF- $\kappa$ B axis to sensitize glioma cells to TNF $\alpha$ -induced apoptosis. *Carcinogenesis* 34, 388–396. <https://doi.org/10.1093/carcin/bgs352>.
- Häcker, H., Karin, M., n.d. Regulation and function of IKK and IKK-related kinases. *Sci. STKE* 2006, re13. <https://doi.org/10.1126/stke.3572006re13>.
- Huang, B., Zhang, H., Gu, L., Ye, B., Jian, Z., Sary, C., Xiong, X., 2017. Advances in immunotherapy for glioblastoma multiforme. *J. Immunol. Res.* 2017, 1–11. <https://doi.org/10.1155/2017/3597613>.
- Islam, F., Gopalan, V., Lam, A.K.Y., Kabir, S.R., 2018. Pea lectin inhibits cell growth by inducing apoptosis in SW480 and SW48 cell lines. *Int. J. Biol. Macromol.* 117, 1050–1057. <https://doi.org/10.1016/j.ijbiomac.2018.06.021>.
- Jiapaer, S., Furuta, T., et al, 2018. Potential strategies overcoming the temozolomide resistance for glioblastoma. *Neurol. Med. Chir.* 58, 405–421. <https://doi.org/10.2176/nmc.ra.2018-0141>.
- Kabir, S.R., Asaduzzaman, A., Amin, R., Haque, A.T., Ghose, R., Rahman, M.M., Islam, J., Amin, M.B., Hasan, I., Debnath, T., Chun, B.-S., Zhao, X., Khan, M.K.R., Alam, M.T., 2020a. Zizyphus mauritiana Fruit Extract-Mediated Synthesized Silver/Silver Chloride Nanoparticles Retain Antimicrobial Activity and Induce Apoptosis in MCF-7 Cells through the Fas Pathway. *ACS Omega* 5, 20599–20608. <https://doi.org/10.1021/acsomega.0c02878>.
- Kabir, S.R., Dai, Z., Nurujjaman, M., Cui, X., Asaduzzaman, A.K.M., Sun, B., Zhang, X., Dai, H., Zhao, X., 2020b. Biogenic silver/silver chloride nanoparticles inhibit human glioblastoma stem cells growth in vitro and Ehrlich ascites carcinoma cell growth in vivo. *J. Cell. Mol. Med.* 24, 13223–13234. <https://doi.org/10.1111/jcmm.15934>.
- Kabir, S.R., Islam, J., Ahamed, M.S., Alam, M.T., 2021. Asparagus racemosus and Geodorum densiflorum lectins induce apoptosis in cancer cells by altering proteins and genes expression. *Int. J. Biol. Macromol.* 191, 646–656. <https://doi.org/10.1016/j.ijbiomac.2021.09.101>.
- Kabir, S.R., Islam, M.F., Alom, M.J., Zubair, M.A., Absar, N., 2012. Purification, Characterizations of a Snake Guard Seeds Lectin with Anti-tumor Activity Against Ehrlich Ascites Carcinoma Cells In Vivo in Mice. *Protein Pept. Lett.* 19, 360–368. <https://doi.org/10.2174/092986612799363154>.
- Kabir, S.R., Rahman, M.M., Amin, R., Karim, M.R., Mahmud, Z.H., Hossain, M.T., 2016. Solanum tuberosum lectin inhibits Ehrlich ascites carcinoma cells growth by inducing apoptosis and G2/M cell cycle arrest. *Tumor Biol.* 37, 8437–8444. <https://doi.org/10.1007/s13277-015-4735-x>.
- Kabir, S.R., Islam, F., Asaduzzaman, A.K.M., 2022. Biogenic silver/silver chloride nanoparticles inhibit human cancer cells proliferation in vitro and Ehrlich ascites carcinoma cells growth in vivo. *Sci. Rep.* 12 (1), 8909. <https://doi.org/10.1038/s41598-022-12974-z>.
- Kaltschmidt, B., Kaltschmidt, C., Hofmann, T.G., Hehner, S.P., Dröge, W., Schmitz, M.L., 2000. The pro- or anti-apoptotic function of NF- $\kappa$ B is determined by the nature of the apoptotic stimulus. *Eur. J. Biochem.* 267, 3828–3835. <https://doi.org/10.1046/j.1432-1327.2000.01421.x>.
- Kang, Y.O., Jung, J.Y., Cho, D., Kwon, O.H., Cheon, J.Y., Park, W. H., 2016. Antimicrobial silver chloride nanoparticles stabilized with chitosan oligomer for the healing of burns. *Materials (Basel)*. 9, 1–10. <https://doi.org/10.3390/ma9040215>.
- Kim, S., Ezhilarasan, R., Phillips, E., Al, E., 2016. Serine/threonine kinase MLK4 determines mesenchymal identity in glioma stem cells in an NF- $\kappa$ B-dependent manner. *Cancer Cell* 29, 201–213. <https://doi.org/10.1016/j.ccell.2016.01.005>.
- Lathia, J.D., Mack, S.C., Mulkearns-Hubert, E.E., Valentim, C.L.L., Rich, J.N., 2015. Cancer stem cells in glioblastoma. *Genes Dev.* 29, 1203–1217. <https://doi.org/10.1101/gad.261982.115>.
- Lee, D.H., Ryu, H.-W., Won, H.-R., Kwon, S.H., 2017. Advances in epigenetic glioblastoma therapy. *Oncotarget* 8, 18577–18589. <https://doi.org/10.18632/oncotarget.14612>.
- Li, Y., Zhou, Q.-L., Sun, W., Chandrasekharan, P., Cheng, H.S., Ying, Z., Lakshmanan, M., Raju, A., Tenen, D.G., Cheng, S.-Y., Chuang, K.-H., Li, J., Prabhakar, S., Li, M., Tergaonkar, V., 2015. Non-canonical NF- $\kappa$ B signalling and ETS1/2 cooperatively drive C250T mutant TERT promoter activation. *Nat. Cell Biol.* 17, 1327–1338. <https://doi.org/10.1038/ncb3240>.
- Lin, B., Williams-Skipp, C., Tao, Y., Schleicher, M.S., Cano, L.L., Duke, R.C., Scheinman, R.I., 1999. NF- $\kappa$ B functions as both a proapoptotic and antiapoptotic regulatory factor within a single cell type. *Cell Death Differ.* 6, 570–582. <https://doi.org/10.1038/sj.cdd.4400528>.
- Louis, D.N., 2006. Molecular pathology of Malignant Gliomas. *Annu. Rev. Pathol. Mech. Dis.* 1, 97–117. <https://doi.org/10.1146/annurev.pathol.1.110304.100043>.
- Medzhitov, R., 2001. Toll-like receptors and innate immunity. *Nat. Rev. Immunol.* 1, 135–145. <https://doi.org/10.1038/35100529>.
- Mitra, S.K., Prakash, N.S., Sundaram, R., 2012. Shatavarins (containing Shatavarin IV) with anticancer activity from the roots of *Asparagus racemosus*. *Indian J. Pharmacol.* 44, 732–736. <https://doi.org/10.4103/0253-7613.103273>.
- Ostrom, Q., Gittleman, H., Fulop, J., ... M.L.-N., 2015, undefined, n. d. CBTRUS statistical report: primary brain and central nervous system tumors diagnosed in the United States in 2008–2012. [academic.oup.com](http://academic.oup.com).

- Ozdemir-Kaynak, E., Qutub, A.A., Yesil-Celiktas, O., 2018. Advances in glioblastoma multiforme treatment: New models for nanoparticle therapy. *Front. Physiol.* <https://doi.org/10.3389/fphys.2018.00170>.
- Padalia, H., Moteriyia, P., Chanda, S., 2015. Green synthesis of silver nanoparticles from marigold flower and its synergistic antimicrobial potential. *Arab. J. Chem.* 8, 732–741. <https://doi.org/10.1016/j.arabjc.2014.11.015>.
- Pasare, C., Medzhitov, R., 2005. Toll-like receptors: Linking innate and adaptive immunity. *Adv. Exp. Med. Biol.*, 11–18 [https://doi.org/10.1007/0-387-24180-9\\_2](https://doi.org/10.1007/0-387-24180-9_2).
- Patial, S., Luo, J., Porter, K.J., Benovic, J.L., Parameswaran, N., 2010. G-protein-coupled-receptor kinases mediate TNF $\alpha$ -induced NF- $\kappa$ B signalling via direct interaction with and phosphorylation of I $\kappa$ B $\alpha$ . *Biochem. J.* 425, 169–180. <https://doi.org/10.1042/BJ20090908>.
- Peng, W., Hegazy, A.M., Jiang, N., Chen, X., Qi, H.X., Zhao, X.D., Pu, J., Ye, R.R., Li, R.T., 2020. Identification of two mitochondrial-targeting cyclometalated iridium(III) complexes as potent anti-glioma stem cells agents. *J. Inorg. Biochem.* 203, <https://doi.org/10.1016/j.jinorgbio.2019.110909> 110909.
- Stupp, R., Hegi, M.E., Mason, W.P., van den Bent, M.J., Taphoorn, M.J.B., Janzer, R.C., Ludwin, S.K., Allgeier, A., Fisher, B., Belanger, K., Hau, P., Brandes, A.A., Gijtenbeek, J., Marosi, C., Vecht, C.J., Mokhtari, K., Wesseling, P., Villa, S., Eisenhauer, E., Gorlia, T., Michael Weller, D.L., Cairncross, J.G., Mirimanoff, R.O., 2009. Effects of Radiotherapy With Concomitant and Adjuvant Temozolomide Versus Radiotherapy Alone on Survival in Glioblastoma in a Randomised Phase III Study: 5-year Analysis of the EORTC-NCIC Trial. *Lancet Oncol.* 10, 459–466. [https://doi.org/10.1016/S1470-2045\(09\)70025-7](https://doi.org/10.1016/S1470-2045(09)70025-7).
- Roosen, N., Kiwit, J.C., Lins, E., Schirmer, M., Bock, W.J., 1989. Adjuvant intraarterial chemotherapy with nimustine in the management of world health organization grade IV gliomas of the brain. *Cancer* 64, 1984–1994. [https://doi.org/10.1002/1097-0142\(19891115\)64:10<1984::aid-cnrcr2820641003>3.0.co;2-s](https://doi.org/10.1002/1097-0142(19891115)64:10<1984::aid-cnrcr2820641003>3.0.co;2-s).
- Sai, K., Wang, S., Balasubramanian, V., Conrad, C., Lang, F.F., Aldape, K., Szymanski, S., Fokt, I., Dasgupta, A., Madden, T., Guan, S., Chen, Z., Yung, W.K.A., Priebe, W., Colman, H., 2012. Induction of cell-cycle arrest and apoptosis in glioblastoma stem-like cells by WP1193, a novel small molecule inhibitor of the JAK2/STAT3 pathway. *J. Neurooncol.* 107, 487–501. <https://doi.org/10.1007/s11060-011-0786-z>.
- Sattiraju, A., Sai, K.K.S., Mintz, A., 2017. Glioblastoma Stem Cells and Their Microenvironment. *Adv. Exp. Med. Biol.* 1041, 119–140. [https://doi.org/10.1007/978-3-319-69194-7\\_7](https://doi.org/10.1007/978-3-319-69194-7_7).
- Sherry, M.M., Reeves, A., Wu, J.K., Cochran, B.H., 2009. STAT3 is required for proliferation and maintenance of multipotency in glioblastoma stem cells. *Stem Cells* 27, 2383–2392. <https://doi.org/10.1002/stem.185>.
- Singh, G., Babele, P.K., Shahi, S.K., Sinha, R.P., Tyagi, M.B., Kumar, A., 2014. Green synthesis of silver nanoparticles using cell extracts of *Anabaena doliolum* and screening of its antibacterial and antitumor activity. *J. Microbiol. Biotechnol.* 24, 1354–1367. <https://doi.org/10.4014/jmb.1405.05003>.
- Thuy, M.N.T., Kam, J.K.T., Lee, G.C.Y., Tao, P.L., Ling, D.Q., Cheng, M., Goh, S.K., Papachristos, A.J., Shukla, L., Wall, K.-L., Smoll, N.R., Jones, J.J., Gikenye, N., Soh, B., Moffat, B., Johnson, N., Drummond, K.J., 2015. A Novel Literature-Based Approach to Identify Genetic and Molecular Predictors of Survival in Glioblastoma Multiforme: Analysis of 14,678 Patients Using Systematic Review and Meta-Analytical Tools. *J. Clin. Neurosci.* 22, 785–799. <https://doi.org/10.1016/j.jocn.2014.10.029>.
- Wang, H., Lathia, J.D., Wu, Q., Wang, J., Li, Z., Heddleston, J.M., Eyler, C.E., Elderbroom, J., Gallagher, J., Schusch, J., MacSwords, J., Cao, Y., McLendon, R.E., Wang, X.F., Hjelmeland, A. B., Rich, J.N., 2009. Targeting interleukin 6 signaling suppresses glioma stem cell survival and tumor growth. *Stem Cells* 27, 2393–2404. <https://doi.org/10.1002/stem.188>.
- Wang, W., Zhao, Z., Wu, F., Wang, H., Wang, J., Lan, Q., Zhao, J., 2018. Bioinformatic analysis of gene expression and methylation regulation in glioblastoma. *J. Neurooncol.* 136, 495–503. <https://doi.org/10.1007/s11060-017-2688-1>.
- Wei, X., Chen, X., Ying, M., Lu, W., 2014. Brain tumor-targeted drug delivery strategies. *Acta Pharm. Sin. B* 4, 193–201. <https://doi.org/10.1016/j.apsb.2014.03.001>.
- Yang, F., Hu, M., Lei, Q., Xia, Y., Zhu, Y., Song, X., Li, Y., Jie, H., Liu, C., Xiong, Y., Zuo, Z., Zeng, A., Yu, L., Shen, G., Wang, D., Xie, Y., Ye, T., Wei, Y., 2015. Nifuroxazide induces apoptosis and impairs pulmonary metastasis in breast cancer model. *Cell Death Dis.* 6, <https://doi.org/10.1038/cddis.2015.63> e1701.
- Yang, F., Liu, X., Liu, Y., Liu, Y., Zhang, C., Wang, Z., Jiang, T., Wang, Y., Wang, Y., 2017. miR-181d/MALT1 regulatory axis attenuates mesenchymal phenotype through NF- $\kappa$ B pathways in glioblastoma. *Cancer Lett.* 396, 1–9. <https://doi.org/10.1016/j.canlet.2017.03.002>.
- Zanotto-Filho, A., Gonçalves, R.M., Klafke, K., de Souza, P.O., Dillenburger, F.C., Carro, L., Gelain, D.P., Moreira, J.C.F., 2017. Inflammatory landscape of human brain tumors reveals an NF $\kappa$ B dependent cytokine pathway associated with mesenchymal glioblastoma. *Cancer Lett.* 390, 176–187. <https://doi.org/10.1016/j.canlet.2016.12.015>.